The Septin Cytoskeleton excludes the Cdc42 GAP Rga4 from growing sites to promote bipolarity in fission yeast

Justin McDuffie, Goeun Chang, Maitreyi Das*

Biology Department, Boston College, Chestnut Hill, MA, 02467

***Corresponding author:** Maitreyi.Das@bc.edu

Running title: Septins restrict Rga4 localization

Keywords: Septin, Cell cycle, Cdc42, GAP, Rga4, Cell polarity

Summary: Cell-cycle-dependent Rga4 localization pattern is controlled by the septin cytoskeleton to promote bipolar growth. In interphase, the septin cytoskeleton at the cell sides restricts Rga4 mobility and localization away from the cell ends to promote proper Cdc42 activation dynamics.

ABSTRACT

The conserved GTPase Cdc42 regulates polarity in most eukaryotes and is spatiotemporally regulated to confine growth to discreet areas throughout the cell cycle. Cdc42 activity stops at the growing ends of fission yeast during mitosis and resumes after division when the ends remove the inactivator/GAP Rga4. In interphase, Rga4 appear punctate at the cell sides restricted from the growing ends. During mitosis, Rga4 appears homogeneous and localizes to the ends. We show that this cell-cycle-dependent Rga4 localization is septin cytoskeleton-dependent. Septins forms linear filaments along the sides during interphase. In mitosis, the septins recede from the sides and form a ring at the division site. In septin mutants, Rga4 is mobile, homogeneously distributed and localizes to the ends, regardless of cell-cycle stage. Accordingly, septin mutants show delayed Cdc42 reactivation after division and are monopolar with disrupted Cdc42 activation dynamics. Our data describe an unusual form of polarity regulation where a septin-dependent physical barrier restricts GAP localization for proper Cdc42 dynamics.

INTRODUCTION

Establishment and maintenance of cell shape is fundamental to its function. Most cells exhibit consistent cell shape after every round of cell division and this ensures their ability to maintain function. Consistent cell shape is not just observed in multicellular organisms that form highly organized tissues and organelles, but even in unicellular organisms such a yeast (Das and Verde, 2013; Galliot and Ghila, 2010; Guillot and Lecuit, 2013; Mitchison and Nurse, 1985). In most eukaryotes, polarized cell growth stops during division and resumes immediately after to establish consistent cell shape (Lloyd, 2013; McCusker and Kellogg, 2012). It is not well understood how polarized growth resumes promptly after each round of cell division. To understand this process, we use the fission yeast model system *Schizosaccharomyces pombe*. These cells stop polarized growth from the cell ends during division and resume growth once the cells complete cytokinesis (Mitchison and Nurse, 1985). However, we have previously shown that resumption of polarized growth from the cell ends is independent of cytokinesis and is instead cell-cycle-dependent and occurs at a fixed time after mitosis (Rich-Robinson et al., 2021).

Like in many eukaryotic cells, the major regulator of polarized growth in fission yeast is the small GTPase Cdc42 (Das and Verde, 2013; Estravis et al., 2012; Etienne-Manneville, 2004; Johnson, 1999). Cdc42 is activated when Guanine nucleotide exchange factors (GEFs) help it bind GTP (Bos et al., 2007; Sprang, 2001). GTP-bound Cdc42 binds and activates downstream targets to promote polarized growth (Bos et al., 2007). Cdc42 is inactivated when it hydrolyses the GTP to GDP with the help of the

56 GTPase activating proteins (GAPs) (Bos et al., 2007). Cdc42 in fission yeast has two
57 GEFs, Scd1 and Gef1, and three GAPs, Rga4, Rga6 and Rga3 (Chang et al., 1994;
58 Coll et al., 2003; Das et al., 2007; Gallo Castro and Martin, 2018; Murray and Johnson,
59 2001; Revilla-Guarinos et al., 2016; Tatebe et al., 2008). Our lab previously showed that
60 during cell division, the GAP Rga4 undergoes a change in its localization pattern (Rich-
61 Robinson et al., 2021). Rga4 localizes to the cell sides in a punctate manner during
62 interphase. It becomes diffuse along the cell cortex and localizes to the cell tips in
63 dividing cells, where it prevents Cdc42 activation. Once cells complete division, Rga4
64 resumes its punctate localization away from the cell ends and growth at the ends
65 resume. It is not known how Rga4 localization is regulated in a cell-cycle-dependent
66 manner.
67
68 Rga4 has a coiled-coil region that is required for its localization to the cell cortex (Das et
69 al., 2007). Cells lacking *rga4* show increased width, since in these mutants, the zone of
70 Cdc42 activation and consequent growth spreads over a larger area at the cell ends
71 (Das et al., 2007; Tatebe et al., 2008). It is not known how Rga4 localization is limited to
72 the cell sides and away from the ends. A recent report shows that Rga4 is removed from
73 the cell ends as a result of membrane flow that occurs due to extensile growth at these
74 ends (Gerganova et al., 2021; Rutkowski et al., 2024). During mitosis, Rga4 appears
75 diffuse along the membrane and appears at the cell ends (Rich-Robinson et al., 2021).
76 It is not known what prevents the diffuse Rga4 localization at the cell surface restricting
77 it to the sides.
78

In several eukaryotic cells the septin cytoskeleton acts as a diffusion barrier along the membrane (Bridges and Gladfelter, 2015; Caudron and Barral, 2009; Kinoshita, 2003). *S. pombe* expresses seven total septin proteins (Spn1-7p), however, only four are involved in the regular cell cycle (Spn1-4p) (An et al., 2004; Berlin et al., 2003; Onishi et al., 2010). The septin cytoskeleton is a heterotetramer consisting of 4 peptides Spn1-4 (An et al., 2004; Berlin et al., 2003). These peptides form heterotetramer that organize in a palindromic manner to form larger filaments (Kinoshita, 2003; Spiliotis and McMurray, 2020; Woods and Gladfelter, 2021). The septin cytoskeleton plays a role in cytokinesis where it forms a ring at the division site during cytokinesis. The septin ring acts as the landmark where proteins required for cell separation during cytokinesis are delivered (Berlin et al., 2003; Maddox et al., 2007; Martin-Cuadrado et al., 2005; Singh et al., 2024; Spiliotis and McMurray, 2020). It is not clear if the septin cytoskeleton plays a role during interphase. Cells lacking the septin cytoskeleton show cell separation defects but remain polarized (An et al., 2004; Berlin et al., 2003; Martin-Cuadrado et al., 2005).

Here we show that the septin cytoskeleton acts as a barrier to prevent Rga4 diffusion along the cell cortex and restrict it to the cell sides. In cells lacking septin filaments, Rga4 localization is diffuse along the cortex and also appears at the cell ends, similar to that observed in mitotic cells. In the presence of septin filaments, the Rga4 puncta at the cell sides are mostly immobile. During interphase, the septin cytoskeleton forms small filaments at the cortex that align along the long axis of the cell. The septin levels along the cortex decrease as the cells enter mitosis, and eventually, a septin ring forms

102 at the end of anaphase B. Rga4 localization appears diffuse as the cells enter mitosis,
103 and throughout cytokinesis. Correspondingly, active Cdc42 is lost from the cell ends
104 during mitosis. Using the GFP-GBP trap method, we show that the septin cytoskeleton
105 does not interact with Rga4 and likely restricts its diffusion by acting as a barrier. The
106 septin mutants show a delay in reactivation of Cdc42 at the cell ends as the cells
107 complete division. Moreover, these mutants are monopolar compared to controls,
108 indicating that the presence of Rga4 at the cells ends disrupts bipolarity. Together, these
109 findings show that the septin cytoskeleton forms a diffusion barrier along the cortex to
110 restrict Rga4 localization along the cell sides. During mitosis, septin localization along
111 the cortex is lost, thus allowing diffusion of Rga4 along the membrane and its
112 localization to the cell ends. Rga4 at the ends in the absence of septin disrupt Cdc42
113 activation dynamics resulting in monopolar cells. These findings show that the septin
114 cytoskeleton maintains cell polarity in a cell-cycle-dependent manner.

RESULTS

The septin cytoskeleton restricts Rga4 to the cell sides during interphase

To investigate if the septin cytoskeleton acts as a diffusion barrier for Rga4, we analyzed Rga4-GFP localization in *spn1*$^{+}$ and *spn1Δ* cells. In the *spn1*$^{+}$ cells, Rga4-GFP along the cell sides appears punctate in interphase cells and diffuse in dividing cells. In contrast, *spn1Δ* cells Rga4-GFP show the diffuse pattern, regardless of the cell cycle stage (Fig.1A). We quantified the level of Rga4 heterogeneity along the cell sides by measuring the coefficient of variance of Rga4-GFP intensity. As reported earlier, we find that the coefficient of variance of Rga4-GFP is highest in the cells in G2 phase of the cell cycle and the lowest in the mitotic phase in *spn1*$^{+}$ cells (Fig 1, B) (Rich-Robinson et al., 2021). This indicates that Rga4-GFP is more homogeneous along the cell sides in mitotic cells and form puncta during G2 or interphase. In *spn1Δ* cells, the coefficient of variance in G2 cells is low and is similar to that in mitotic cells (Fig 1, C).

In mitotic, cells Rga4 appears more cytoplasmic and is also increasingly observed at the cell ends. We asked if septins restrict cytoplasmic Rga4 and prevents its localization to the cell ends. Rga4-GFP along the cells ends appear faint even in z-projected images due to the curvature of the cell and weak expression/signal. To overcome this, we took rapid timelapse movies with 5 second intervals over 5 mins of Rga4-GFP expressing *spn1*+ and *spn1Δ* cells. We measured Rga4-GFP intensity in the cytoplasm and the cell ends of time-projected images of these movies (Fig1, D). We find that compared to *spn1*$^{+}$ cells cytoplasmic Rga4-GFP levels increase in *spn1Δ* cells (Fig1, E). Similarly, *spn1Δ* cells show enhanced Rga4-GFP levels at the cell ends compared to *spn1*$^{+}$ cells (Fig1, F). In control cells, Rga4-GFP shows elevated levels at the non-growing cell ends

138 compared to growing ends. We also see higher levels of Rga4-GFP at the non-growing
139 cell ends of *spn1Δ* cells but these levels are much higher than that in *spn1*+ cells.
140 Moreover, the growing ends in *spn1Δ* cells show higher Rga4-GFP levels compared to
141 growing ends of *spn1*$^{+}$ cells. This indicates that in the absence of septins, Rga4-GFP
142 levels at the cell ends are elevated.

143 **Septins inhibit Rga4-GFP mobility during Interphase**

144

145 Next, we asked whether the increased homogeneity of Rga4-GFP along the plasma
146 membrane is the result of increased Rga4-GFP mobility or diffusion along the
147 membrane. The above mentioned 5-minute timelapse movies of Rga4-GFP localization
148 were analyzed and we found that, in *spn1*$^{+}$ cells in interphase, Rga4-GFP formed a
149 number of bright, stationary puncta along the plasma membrane that remained
150 immobile throughout the course of timelapse imaging (Fig. 2A). In contrast, *spn1*$^{+}$ cells
151 in mitosis, and *spn1Δ* cells at all stages of the cell-cycle showed limited Rga4-GFP
152 puncta formation, and lacked immobile Rga4-GFP puncta. In these cells Rga4-GFP
153 appeared to diffuse more rapidly along the plasma membrane. To quantify this observed
154 change in Rga4 mobility, fluorescence recovery after photobleaching (FRAP)
155 microscopy was performed on 10x10-pixel ROIs of Rga4-GFP along the cell sides of
156 *spn1*$^{+}$ and *spn1Δ* cells in interphase and mitosis (Fig. 2B). Cell-cycle-progression was
157 marked by the fluorescently tagged spindle pole body marker Sad1-mCherry.
158 Fluorescence recovery curves and calculated recovery half-lives of Rga4-GFP in the
159 photobleached ROIs showed that Rga4-GFP was much less mobile along the plasma
160 membrane in interphase cells (Fig. 2C, D). In contrast, Rga4-GFP is much more mobile
161 along the plasma membrane in *spn1*$^{+}$ cells during mitosis. Similarly, to mitotic *spn1*$^{+}$
162 cells, Rga4-GFP is much more mobile along the plasma membrane in *spn1Δ* cells,
163 regardless of cell-cycle-stage. This indicates that in the absence of septin filaments, the
164 diffusion of Rga4-GFP is significantly less restricted than when they are present, leading
165 to increased protein mobility. This increased mobility along the plasma membrane may

166 also explain the increased localization of Rga4-GFP to the cytoplasm and the cell ends
167 in the septin mutants.
168
169 A previous report has indicated that the GAP Rga6 interacts with the septin filaments
170 and is required for proper septin localization at the cortex in interphase cells (Zheng et
171 al., 2022). Thus, we asked if the septin filaments also regulate Rga6 distribution along
172 the cortex. Similar to Rga4-GFP, Rga6-GFP also appears punctate along the cell sides
173 (Supplementary Fig. S1A). However, in *spn1Δ* mutants, Rga6-GFP localization
174 remained the same and the coefficient of variance along the cortex was not significantly
175 distinct between *spn1*$^{+}$ and *spn1Δ* cells, and throughout the cell cycle stages
176 (Supplementary Fig. S1B). This indicates that the septin cytoskeleton specifically
177 disrupts Rga4 distribution along the cortex.

178 **Septins form linear filaments in interphase and a ring structure as Anaphase B**
179 **ends**

180 Given that Rga4-GFP localization in *spn1Δ* cells regardless of the cell cycle stage is
181 similar to that of mitotic *spn1*$^{+}$ cells, we asked if this is due to changes in septin
182 localization throughout the cell cycle. While extensive work has revealed septin
183 localization at the division site during cytokinesis, it is unclear how septin proteins
184 localize during interphase. We find that in interphase cells, the septin proteins appear as
185 short filaments at the plasma membrane along the long axis of the cell. Spn1-tdTomato
186 and Spn3-GFP co-localize as short linear filaments along the cell cortex (Fig 3A). The
187 other septin protein Spn2 also appears as short filaments along the long axis of the cell
188 as determined by Spn2-GFP (Fig. 3B). Spn4 on the other hand appears more punctate
189 but along the cell sides as determined by Spn4-tdTomato (Fig.3C).
190

191 The septin filament distribution appears biased towards the growing cell ends. To
192 confirm this, we investigated Spn3-GFP localization in *tea1*+ and *tea1Δ* mutants. The
193 *tea1Δ* mutants are monopolar and only grow from one end (Mata and Nurse, 1997;
194 Verde et al., 1995). We find that in *tea1Δ* cells Spn3-GFP filaments appear closer to the
195 growing cell ends (Supplementary Fig. S2A, red arrowheads). In *tea1Δ* cells Spn3-GFP
196 levels are higher at the growing ends compared to the *tea1*+ cells (Supplementary Fig.
197 S2B). This is likely due to the fact that in *tea1*+ cells Spn3-GFP is distributed between
198 the two growing ends of bipolar cells while in *tea1Δ* cells all of the Spn3-GFP
199 accumulates to the single growing end.
200

201 Since, the septin cytoskeleton appears to restrict Rga4 mobility, we asked of the septin
202 proteins themselves were mobile along the cell cortex. To test for mobility, we performed
203 FRAP analysis of Spn1-tdTomato along the cell sides in both interphase and dividing
204 cells. Regardless of the cell cycle stage, we do not see any recovery of the fluorescent
205 signal after photobleaching of Spn1-tdTomato (Supplementary Fig. S2C,D). This
206 indicates that the septin filaments observed along the cell sides are stable and
207 immobile.
208
209 Next, we investigated how septin localization changes throughout the cell cycle. We
210 imaged cells expressing Spn4-tdTomato along with Myo2-GFP and Sid4-GFP over
211 timelapse (Fig. 3D). While the Sid4-GFP labels the spindle pole body and determines
212 the onset of mitosis when the spindle pole body splits into two, Myo2-GFP labels the
213 cytokinetic actomyosin ring (Sparks et al., 1999; Wei et al., 2017). We find that Spn4-
214 tdTomato intensity along the cell cortex starts to drop as the cell enters mitosis, until it
215 plateaus (Fig.3E). The Spn4-tdTomato eventually forms a septin ring just prior to mitotic
216 exit. We quantified Spn4-tdTomato levels along the sides of cells in different mitotic
217 stages, as determined by the distance between spindle pole bodies. We find that Spn4-
218 tdTomato levels along the cell sides is highest in interphase cells with a single spindle
219 pole body (distance, 0μm, Fig. 3F). As the spindle pole body distance increases, Spn4-
220 tdTomato levels along the cell sides drop. Together these observations indicate that, in
221 interphase cells, septins form short linear filaments at the cortex along the long axis of
222 the cell. These filaments begin to drop when the cell enters mitosis, however the septin
223 ring forms after a delay close to the end of Anaphase B.

224 **The septin cytoskeleton and Rga4 show distinct structures at the cortex**

225 Since Rga4 distribution pattern along the cortex is septin-dependent, we investigated
226 whether the septin cytoskeleton colocalizes with Rga4. We observed Rga4-GFP puncta
227 along the cell sides in cells expressing Spn1-tdTomato. While both these proteins
228 localize to the cell sides, we did not see any significant colocalization pattern between
229 them (Fig.4A, Top plane, inset). In most cells, Rga4-GFP organizes like a corset at the
230 cell middle as has been reported before, while Spn1-tdTomato appears on either side of
231 Rga4-GFP closer to the growing ends (Fig.4A, red arrowhead). In some cells, Rga4-
232 GFP puncta appeared on either side of Spn1-tdTomato filaments (Fig.4A, middle plane,
233 inset). We asked if the dynamic Rga4-GFP is trapped by the septin via physical
234 interaction, thereby preventing its mobility along the cortex.

235

236 If the septin cytoskeleton physically interacts with Rga4 and entraps it, mislocalizing the
237 septin should lead to Rga4-GFP mislocalization. To test this, we used the GFP trap
238 method with a GFP-binding protein (GBP) (Wang et al., 2016). We used the
239 mitochondrial protein Tom20 tagged with GBP and RFP to entrap Spn3-GFP (Fig.4B).
240 We find that in cells expressing Tom20-GBP-RFP, Spn3-GFP is no longer observed at
241 the cortex and rather appears along the mitochondria colocalizing with Tom20. We
242 asked if mislocalizing one of the components of the septin cytoskeleton can mislocalize
243 the other components. We expressed Spn1-TdTomato and Spn3-GFP in cells
244 expressing Tom20-GBP. We find that Spn3-GFP with Tom20-GBP at the mitochondria
245 also entraps Spn1-tdTomato at that site (Fig.4C). This indicates that the septin
246 cytoskeleton is mislocalized to the mitochondria with Tom20-GBP.

247 Next, we asked if Rga4-GFP can be mislocalized to the mitochondria with Tom20-GBP.
248 We find that in cells expressing Tom20-GBP, Rga4-GFP appears away from the cortex
249 and along the mitochondria (Fig.4D). However, in these cells Spn1-tdTomato remained
250 at the cortex and did not colocalize with the mitochondria and Rga4-GFP. Moreover, in
251 Tom20-GBP expressing cells, Spn3-GFP at the mitochondria did not entrap Rga4-
252 mCherry (Fig.4D). In these cells, Rga4-mCherry remained at the cortex along the cell
253 sides. These observations suggest that the septin cytoskeleton does not regulate Rga4
254 distribution via physical interaction.
255
256 It is noteworthy that in the cells where the septin cytoskeleton localized to the
257 mitochondria and away from the cortex, Rga4 at the cell sides appeared less punctate
258 and more diffuse, similar to that observed in *spn1Δ* cells. To confirm this, we quantified
259 the coefficient of variance of Rga4-mCherry signal along the cell sides in control cells
260 with that of cells co-expressing Tom20-GBP and Spn3-GFP. We find that the coefficient
261 of variance of Rga4-mCherry is significantly reduced in cells where Spn3-GFP is
262 mislocalized to the Tom20-GBP containing mitochondria (Fig.4F). This indicates that the
263 absence of the septin cytoskeleton from the cell cortex is sufficient to alter Rga4
264 distribution pattern even in cells where the septin proteins are expressed. These
265 observations further support the hypothesis that the septin cytoskeleton acts as a
266 physical barrier that prevents Rga4 mobility along the cell sides.

267 **As septins recede from the cell sides, Rga4 spreads out along the membrane and**
268 **Cdc42 activity diminishes at the cell ends**
269 Our data show that Rga4 localization at the cortex is mostly punctate and immobile in
270 interphase and diffused and mobile in dividing cells. In addition, we find that the septins
271 show short filaments along the cell cortex in interphase and this localization is lost once
272 the cell enters mitosis. Based on this, we propose that Rga4 diffuses along the cortex
273 when the septins are lost from this region. To verify this, we observed Rga4-GFP and
274 Spn1-tdTomato localization along the cortex in cells at different cell cycle stages
275 (Supplementary Fig.S2E). As expected, we find that in early and late G2 cells Rga4-
276 GFP appears punctate along the cell sides. Spn1-tdTomato also localizes to this region.
277 In early and late mitotic cells, Rga4-GFP appears more diffuse and Spn1-tdTomato
278 levels along the sides is lower. Given the low levels of Rga4, it was not possible to
279 image Rga4-GFP through timelapse of different cell cycle stages along with Spn1-
280 tdTomato. The Spn1-tdTomato ring appears in post-mitotic cells while Rga4-GFP shows
281 diffuse localization in mitotic cells as the septin localization along the cortex decreases
282 (Supplementary Fig.S2E, early and late mitosis). This suggests that the removal of
283 septins from the cell cortex, and not the formation of the septin ring, is sufficient to
284 enable diffuse Rga4 localization.
285
286 Next, we asked if Rga4 mobility and its ability to localize to the cell ends leads to Cdc42
287 inactivation at the cell ends in dividing cells. We find that active Cdc42 at the cell ends is
288 not immediately lost upon the onset of mitosis, as observed in CRIB-mCherry
289 expressing cells with Sad1-mCherry as spindle pole body markers (Supplementary

290 Fig.S2F). As the Rga4-GFP appears diffuse in these cells during mitosis, we observe
291 loss of CRIB-mCherry from the ends. This suggests that as the septins gradually
292 decrease from the cell sides, Rga4 mobility along the cortex is enhanced, resulting in
293 eventual loss of active Cdc42 from the cell ends.
294 Cdc42 is active at the cell ends in interphase and at the division site in diving cells
295 (Merla and Johnson, 2000; Wei et al., 2016). Our previous data show that Cdc42
296 activation is lost at the ends during mitosis and is activated at the division site when the
297 cell forms the cytokinetic actomyosin ring. Moreover, delaying Cdc42 activation at the
298 division site did not change the timing of Cdc42 inactivation at the cell ends (Wei et al.,
299 2016). This indicates that Cdc42 inactivation at the ends is independent of its activation
300 at the division site. We analyzed the timing of CRIB-mCherry loss from the cell ends
301 with respect to mitotic progression, as indicated by Sad1-mCherry and changes in
302 Septin Spn3-GFP localization (Fig. 5A). We find that CRIB-mCherry is lost from the cell
303 ends about 10-20 minutes after the onset of mitosis. In contrast the septin ring forms at
304 the end of Anaphase B (Fig.5C). This indicates that as the cells enter mitosis, septin
305 levels at the cell sides drop, allowing Rga4 mobility, which coincides with the loss of
306 active Cdc42 from the cell ends.
307 Our previous report showed that Cdc42 is reactivated at the cell ends as cytokinesis
308 completes to enable old end growth (Rich-Robinson et al., 2021). We asked if Cdc42
309 reactivation at the ends is delayed in *spn1Δ* mutants. Indeed, we find that in *spn1*$^{+}$ cells
310 Cdc42 is reactivated at the cell ends about 10 minutes after the completion of
311 actomyosin ring constriction as indicated by the probe CRIB-3xGFP and ring marker
312 Rlc1-tdTomaton (Fig.5B,D). In *spn1Δ* mutants, Cdc42 reactivation at the ends occurs

313 later, about 15 minutes after the completion of actomyosin ring constriction (Fig.5B,D).

314 This suggests that Cdc42 activity at the cell ends is disrupted in the absence of the

315 septin cytoskeleton.

316 **Septins promote proper cell dimensions and bipolarity**

317 Our data suggest that loss of septins from the cell cortex results in Rga4-mediated
318 inactivation of Cdc42 at the cell ends during mitosis. However, in *rga4Δ* mutants, we do
319 not see any significant change in Cdc42 reactivation at the cell ends during mitosis
320 (data not shown). However, these results were not unexpected, since we have
321 previously shown that precocious Cdc42 activity and consequent polarized growth at
322 the cell ends requires both the loss of *rga4*, and the activation of the MOR/Orb6
323 pathway (Gupta et al., 2014; Ray et al., 2010; Rich-Robinson et al., 2021). Thus, we
324 asked if septin-mediated Rga4 localization plays an important role at the cell ends
325 during interphase.

326

327 Our data show that in *spn1Δ* cells, the ends show increased Rga4-GFP levels, even at
328 the growing cell ends (Fig.1F). Thus, we asked of the presence of Rga4 at the cell ends
329 disrupts Cdc42 dynamics at these ends. We find that *spn1Δ* cells are more monopolar
330 than *spn1*$^{+}$ cells (Fig.6A,B). In addition, *spn1Δ* cells also showed an increase in cell
331 width (Fig. 6A,C). We asked if the increase in cell width was due to an increase in active
332 Cdc42 levels or its distribution at the growing cell ends. We find that compared to *spn1*$^{+}$
333 cells, *spn1Δ* mutants show increased CRIB-GFP levels at the growing ends (Fig.6D,E).
334 In addition, the *spn1Δ* mutants also show an increase in the zone of distribution of
335 CRIB-GFP at the growing ends (Fig.6D,F). An analysis of CRIB-GFP fraction at the
336 ends of *spn1*$^{+}$ cells, appears symmetric between the two ends as the cells increase in
337 size beyond 9μm (Fig.6G). However, in *spn1Δ* cells, the ends show increased
338 asymmetry of the CRIB-GFP fraction between the two cell ends, and symmetry is

339 partially achieved only at a much higher cell length, beyond 11µm, just before the cells
340 start to divide (Fig.6G). Next, we analyzed the localization patterns of the Cdc42 GEF
341 Scd1 and its scaffold protein Scd2. We find that compared to *spn1*$^{+}$ cells, *spn1Δ*
342 mutants show increased levels of Scd1-mNeonGreen and Scd2-GFP levels at the
343 growing cell ends (Fig. 6 H-K). These data suggest that in the absence of the septin
344 cytoskeleton, Cdc42 activation dynamics between the two ends is disrupted and
345 accumulates only at one end, resulting in monopolarity and increased cell width. Thus,
346 we analyzed Cdc42 activation dynamics at the cell ends using the CRIB-3xGFP probe
347 in *spn1*$^{+}$ and *spn1Δ* cells. As reported earlier, CRIB-3xGFP shows anticorrelated
348 oscillations between the two cell ends in control cells (Das et al., 2012). However, in
349 *spn1Δ* cells, CRIB-3xGFP activity fluctuated only at the growing end, while the non-
350 growing end barely showed any signal. This indicates that the septin cytoskeleton is
351 required for proper Cdc42 activation dynamics between the two cell ends.

352 **Discussion**

353 Our previous report showed that Cdc42 activation at the cell ends is cell-cycle-
354 dependent and is turned off during cell division (Rich-Robinson et al., 2021). Cdc42
355 reactivation at the cell ends depends on the activation of the MOR/Orb6 kinase pathway
356 and absence of Rga4 from the cell ends (Gupta et al., 2014; Rich-Robinson et al.,
357 2021). Here we show that cell-cycle-dependent Rga4 localization is dependent on the
358 septin cytoskeleton. The septin cytoskeleton at the cell sides prevents lateral diffusion of
359 Rga4 along the membrane and keeps it away from the cell ends where Cdc42 is
360 activated for polarized growth. Once the cell enters mitosis, the septin cytoskeleton
361 gradually drops from the cell sides and this corresponds with Rga4 diffused localization
362 to the cell ends where Cdc42 is gradually inactivated.

363

364 After division in fission yeast, cells grow in a monopolar manner from old end and
365 transition to bipolar growth when the new end takes off (NETO) (Mitchison and Nurse,
366 1985). Bipolar growth occurs when the old and new ends are able to compete with each
367 other Cdc42 activation (Das et al., 2012). The zone of growth at the cell ends is
368 determined by the Cdc42 activation dynamics and the GAP Rga4 (Das et al., 2012; Das
369 et al., 2007). Rga4 localizes to the cell sides like a corset and prevents the overflow of
370 Cdc42 activation from the ends to these regions. This helps to maintain the cell width
371 and proper polarity. During cell division, Rga4 localizes to the ingressing septum and
372 prevent excessive Cdc42 activation at that site (Campbell et al., 2022). While Rga4 is
373 not present at the growing cell ends, in pre-NETO cells, Rga4 localizes to the non-
374 growing ends. Recent reports show that Rga4 does not localize to the growing cell ends

375 due to plasma membrane flows as a result of growth (Gerganova et al., 2021;
376 Rutkowski et al., 2024). Thus, non-growing ends show Rga4 given the lack of
377 membrane flow at these ends. We find that in cells lacking the septin cytoskeleton,
378 Rga4 levels at both the cell ends increase. This increase is due to the increased
379 mobility of Rga4 along the membrane. However, the levels at the non-growing ends are
380 higher than that at the growing ends, which again can be explained by the effect of
381 growth-dependent membrane flows. In these mutants, the cell ends receive increased
382 levels of Rga4 due to diffusion, while the growth dependent membrane flow removes
383 Rga4. This explains why the Rga4 levels at these ends are not as high as that observed
384 at the cell sides but sufficient to disrupt Cdc42 activation.
385
386 Cdc42 activation dynamics at the cell ends depend on positive and time-delayed
387 negative feedbacks (Das et al., 2012; Harrell et al., 2024; Howell et al., 2012). These
388 feedbacks ensure that the two cell ends can sequentially activate Cdc42 to promote
389 bipolar growth. Previous reports from our lab have shown that the GEF Gef1 is required
390 for establishment of Cdc42 activation at the new end and thus promote bipolar growth
391 (Hercyk and Das, 2019; Hercyk et al., 2019). Any disruption in the Cdc42 activation
392 pattern results in its accumulation at one end at the expense of the other (Das et al.,
393 2012; Harrell et al., 2024). We also observe this in the septin mutants, where Cdc42
394 dynamics is disrupted, resulting in monopolar growth. The low levels of Rga4 at the cell
395 ends can alter the dynamics of Cdc42 activation and inactivation such that it
396 accumulates at one end.
397

398 Our data suggest that the septin cytoskeleton does not restrict Rga4 diffusion via
399 protein-protein interaction. This is in agreement with previous reports that show that the
400 septin cytoskeleton forms a physical barrier on the membrane (Spiliotis and McMurray,
401 2020). The septin filaments at the cell sides are organized along the long axis of the cell
402 while Rga4 on the membrane is organized in small puncta. The Rga4 puncta are mostly
403 distinct from the septin filaments. It is unclear how the septin filaments block Rga4
404 mobility given that these proteins do not colocalize. One possibility is that the septins
405 organize the lipid compartments on the plasma membrane as has been reported in
406 other systems, and this regulates Rga4 localization (Caudron and Barral, 2009). Indeed,
407 Rga4 protein contains a coiled-coil domain that is required for membrane localization
408 (Das et al., 2007). It is possible that the septin cytoskeleton regulates the plasma
409 membrane organization, which indirectly restricts Rga4 diffusion. We are currently
410 investigating whether membrane interactions mediate septin-dependent Rga4
411 localization.
412
413 The septin cytoskeleton in fission yeast has been investigated mostly in the context of
414 cytokinesis (An et al., 2004; Berlin et al., 2003; Martin-Cuadrado et al., 2005; Munoz et
415 al., 2014; Singh et al., 2024; Wang et al., 2015). In budding yeast, the septins organize
416 as a collar around the bud neck and forms a ring during cytokinesis (Bridges and
417 Gladfelter, 2015; Woods and Gladfelter, 2021). The Septin collar in budding yeast has
418 been shown to restrict GAP localization near the bud neck to promote bud emergence
419 for daughter cell formation (Okada et al., 2013). This indicates that restricting GAP
420 localization by septin filaments is a conserved phenomenon. In fission yeast, the septin

421 ring forms as anaphase B ends, when the actomyosin ring starts to constrict. However,
422 the septin filament at the cell sides begin to disappear at the onset of mitosis, well
423 before the septin ring forms. The septin proteins have membrane-interacting domains
424 and are involved in lipid metabolism (Mela and Momany, 2022; Spiliotis and McMurray,
425 2020; Woods and Gladfelter, 2021). It is possible that a mitotic signal disables the
426 septin-membrane interaction resulting in its loss from the cell sides. Further
427 investigation will determine what leads to the loss of septins from the cell sides in
428 mitosis and its subsequent ring formation.
429
430 Our findings here show a role for the septin cytoskeleton in regulating polarized cell
431 growth in a cell-cycle-dependent manner. While most cell cycle dependent regulation is
432 mediated via kinase-substrate phosphorylation (Kaldis, 1999; Malumbres, 2014;
433 McCusker and Kellogg, 2012), here we show a regulatory system where a physical
434 barrier by the septins blocks Rga4 mobility, thereby regulating Cdc42 activation
435 dynamics. While the septin rings have been mostly identified in fungal cells, it is
436 possible that septins in other eukaryotes also undergo cell-cycle-dependent changes in
437 their organization (Delic et al., 2024; Marquardt et al., 2021). In several eukaryotes,
438 septins have been shown to act as diffusion barriers and maintain asymmetry in the cell
439 (Caudron and Barral, 2009). Thus cell-cycle-dependent changes in septin organization
440 may alter their ability to act as barriers. Further, investigation will shed light on the
441 significance of cell-cycle-dependent septin organization and its role in polarity
442 maintenance.

443 **Methods and Materials**

444 **Cell Culture**

445 The *S. pombe* strains used in this study are listed in Table 1. Cells were cultured in
446 yeast extract with supplements (YES – Sunrise Science Products) medium and grown
447 exponentially at 25°C, unless specified otherwise. Standard techniques were used for
448 genetic manipulation and analysis (Moreno et al., 1991). Cells were grown exponentially
449 for at least three rounds of eight generations each before imaging.

450

451 **Microscopy**

452 Imaging was performed at room temperature (23–25°C). We used a spinning disk
453 confocal microscope system with a Nikon Eclipse inverted microscope with a 100×/1.49
454 NA lens, a CSU-22 spinning disk system (Yokogawa Electric Corporation) and a
455 Photometrics EM-CCD camera (Photometrics Technology Evolve with excelon Serial
456 No: A13B107000). Images were acquired with MetaMorph (Molecular Devices,
457 Sunnyvale, CA).

458 A Nikon Ti2 Eclipse wide field microscope was also used with a 100x/1.49 NA objective,
459 an ORCA-FusionBT digital camera (Hamamatsu Model: C15440-20UP Serial No:
460 500428, Hamamatsu, Hamamatsu City, Japan). Images were acquired using Nikon NIS
461 Elements (Nikon, Melville, NY). Fluorophores were excited using an AURA Light Engine
462 system (Lumencor, Beaverton, OR).

463 Additionally, microscopy was performed with a 3i spinning disk confocal using a Zeiss
464 AxioObserver microscope with integrated Yokogawa spinning disk (Yokogawa CSU-X1
465 A1 spinning disk scanner) and a 100x/1.49 NA objective. Images were acquired with a
466 Teledyne Photometrics Prime 95b back-illuminated sCMOS camera (Serial No:
467 A20D203014, Tucson, AZ). Images were acquired using SlideBook (3i Intelligent
468 Imaging innovations, Denver, CO).

469

470 **Fluorescence Intensity Acquisition & Quantification**

471 Image analysis was performed on a Macintosh computer using the public domain NIH
472 Image program (developed at the U.S. National Institutes of Health and available on the
473 Internet at http://rsb.info.nih.gov/nih-image/). Images were acquired at either single,
474 mid-section focal planes, or as Z-stacks with 0.2-0.4 μm focal plane intervals. Z-stack
475 images were superimposed using sum projection for analysis. Mean intensity
476 measurements were used for analysis, along with integrated density values where
477 specified. Prior to intensity acquisition, a region of interest devoid of cells was used for
478 background subtraction. Cell side coefficient of variation measurements were acquired
479 using the segmented line tool on both cell sides. Plot profiles of these lines were
480 generated, and the coefficient of variation was determined via ratio of the standard
481 deviation of intensity values along these lines, divided by each position's average
482 intensity along said line. Cell end intensities were measured using freehand ROIs of
483 sum projected Z-stacks.

484

485 **Fluorescence recovery after photobleaching**

486 Fluorescence recovery after photobleaching (FRAP) was performed as described
487 before (Onwubiko et al., 2019). Fluorescently tagged proteins along the cell cortex were
488 first focused at the medial z-plane and an ROI was selected for bleaching. The ROI was
489 imaged 10 times pre-bleaching and then bleached for 10 s and images were then
490 acquired every 3 s for 50–100 images. A non-bleached spot on the cortex for the same
491 cell was analyzed to account for loss of signal due to photobleaching over time. A cell-
492 free region of the image was used for background subtraction. Intensity values for each
493 ROI were corrected for loss of signal over time and background signal. The intensity
494 values were then normalized against the mean pre-bleach value to determine the
495 recovery fraction over time. At least ten cells were analyzed for each genotype for each
496 experiment in carried out triplicate. The average corrected and normalized intensity
497 values were then plotted as fraction of recovery over time. The fraction of recovery over
498 time was plotted and smoothened using GraphPad *Prism*. The half-life (t1/2) was then
499 computed as time for recovery of 50% of the signal.

Supplemental information titles and legends

Document S1. Figures S1–S3 and Table S1

Data Availability

The data generated are available in the published article and its online supplemental material.

Acknowledgements

We thank Kathy Gould, Fulvia Verde, Pilar Perez and Chuanhai Fu for providing strains and Bret Judson at the Boston College Imaging Core for imaging support. This work is supported by the National Institutes of Health grant R01GM136847 to M.D.

Author contributions

Conceptualization: M.D. and J.M.; Methodology: M.D. and J.M.; Validation: M.D. and J.M.; Formal analysis: M.D. and J.M.; Investigation: M.D., J.M., G.C.; Resources: M.D.; Data curation: J.M. and G.C.; Writing- original draft: M.D. and J.M. ; Writing - review & editing: M.D.; Supervision: M.D.; Project administration: M.D.; Funding acquisition: M.D.

Declaration of interests

The authors declare no competing or financial interests.

521 **References**
522
523 An, H., J.L. Morrell, J.L. Jennings, A.J. Link, and K.L. Gould. 2004. Requirements of
524 fission yeast septins for complex formation, localization, and function. *Molecular*
525 *biology of the cell*. 15:5551-5564.

526 Berlin, A., A. Paoletti, and F. Chang. 2003. Mid2p stabilizes septin rings during
527 cytokinesis in fission yeast. *The Journal of cell biology*. 160:1083-1092.

528 Bos, J.L., H. Rehmann, and A. Wittinghofer. 2007. GEFs and GAPs: critical elements in
529 the control of small G proteins. *Cell*. 129:865-877.

530 Bridges, A.A., and A.S. Gladfelter. 2015. Septin Form and Function at the Cell Cortex.
531 *The Journal of biological chemistry*. 290:17173-17180.

532 Campbell, B.F., B.S. Hercyk, A.R. Williams, E. San Miguel, H.G. Young, and M.E. Das.
533 2022. Cdc42 GTPase activating proteins Rga4 and Rga6 coordinate septum
534 synthesis and membrane trafficking at the division plane during cytokinesis.
535 *Traffic*. 23:478-495.

536 Caudron, F., and Y. Barral. 2009. Septins and the lateral compartmentalization of
537 eukaryotic membranes. *Developmental cell*. 16:493-506.

538 Chang, E.C., M. Barr, Y. Wang, V. Jung, H.P. Xu, and M.H. Wigler. 1994. Cooperative
539 interaction of S. pombe proteins required for mating and morphogenesis. *Cell*.
540 79:131-141.

541 Coll, P.M., Y. Trillo, A. Ametzazurra, and P. Perez. 2003. Gef1p, a new guanine
542 nucleotide exchange factor for Cdc42p, regulates polarity in
543 Schizosaccharomyces pombe. *Molecular biology of the cell*. 14:313-323.

544 Das, M., T. Drake, D.J. Wiley, P. Buchwald, D. Vavylonis, and F. Verde. 2012. Oscillatory
545 Dynamics of Cdc42 GTPase in the Control of Polarized Growth. *Science*.
546 337:239-243.

547 Das, M., and F. Verde. 2013. Role of Cdc42 dynamics in the control of fission yeast cell
548 polarization. *Biochemical Society transactions*. 41:1745-1749.

549 Das, M., D.J. Wiley, S. Medina, H.A. Vincent, M. Larrea, A. Oriolo, and F. Verde. 2007.
550 Regulation of cell diameter, For3p localization, and cell symmetry by fission yeast
551 Rho-GAP Rga4p. *Molecular biology of the cell*. 18:2090-2101.

552 Delic, S., B. Shuman, S. Lee, S. Bahmanyar, M. Momany, and M. Onishi. 2024. The
553 evolutionary origins and ancestral features of septins. *Front Cell Dev Biol*.
554 12:1406966.

555 Estravis, M., S. Rincon, and P. Perez. 2012. Cdc42 regulation of polarized traffic in
556 fission yeast. *Communicative & integrative biology*. 5:370-373.

557 Etienne-Manneville, S. 2004. Cdc42--the centre of polarity. *Journal of cell science*.
558 117:1291-1300.

559 Galliot, B., and L. Ghila. 2010. Cell plasticity in homeostasis and regeneration. *Mol*
560 *Reprod Dev*. 77:837-855.

561 Gallo Castro, D., and S.G. Martin. 2018. Differential GAP requirement for Cdc42-GTP
562 polarization during proliferation and sexual reproduction. *The Journal of cell*
563 *biology*. 217:4215-4229.

564 Gerganova, V., I. Lamas, D.M. Rutkowski, A. Vjestica, D.G. Castro, V. Vincenzetti, D.
565 Vavylonis, and S.G. Martin. 2021. Cell patterning by secretion-induced plasma
566 membrane flows. *Sci Adv*. 7:eabg6718.

567 Guillot, C., and T. Lecuit. 2013. Mechanics of epithelial tissue homeostasis and
568 morphogenesis. *Science*. 340:1185-1189.

569 Gupta, S., M. Govindaraghavan, and D. McCollum. 2014. Cross talk between NDR
570 kinase pathways coordinates cytokinesis with cell separation in
571 Schizosaccharomyces pombe. *Eukaryotic cell*. 13:1104-1112.

572 Harrell, M.A., Z. Liu, B.F. Campbell, O. Chinsen, T. Hong, and M. Das. 2024. Arp2/3-
573 dependent endocytosis ensures Cdc42 oscillations by removing Pak1-mediated
574 negative feedback. *The Journal of cell biology*. 223.

575 Hercyk, B.S., and M.E. Das. 2019. F-BAR Cdc15 Promotes Cdc42 Activation During
576 Cytokinesis and Cell Polarization in Schizosaccharomyces pombe. *Genetics*.
577 213:1341-1356.

578 Hercyk, B.S., J. Rich-Robinson, A.S. Mitoubsi, M.A. Harrell, and M.E. Das. 2019. A
579 novel interplay between GEFs orchestrates Cdc42 activity during cell polarity and
580 cytokinesis in fission yeast. *Journal of cell science*. 132.

581 Howell, A.S., M. Jin, C.F. Wu, T.R. Zyla, T.C. Elston, and D.J. Lew. 2012. Negative
582 feedback enhances robustness in the yeast polarity establishment circuit. *Cell*.
583 149:322-333.

584 Johnson, D.I. 1999. Cdc42: An essential Rho-type GTPase controlling eukaryotic cell
585 polarity. *Microbiology and molecular biology reviews : MMBR*. 63:54-105.

586 Kaldis, P. 1999. The cdk-activating kinase (CAK): from yeast to mammals. *Cellular and*
587 *molecular life sciences : CMLS*. 55:284-296.

588 Kinoshita, M. 2003. The septins. *Genome Biol*. 4:236.

589 Lloyd, A.C. 2013. The regulation of cell size. *Cell*. 154:1194-1205.

590 Maddox, A.S., L. Lewellyn, A. Desai, and K. Oegema. 2007. Anillin and the septins
591 promote asymmetric ingression of the cytokinetic furrow. *Developmental cell*.
592 12:827-835.

593 Malumbres, M. 2014. Cyclin-dependent kinases. *Genome Biol*. 15:122.

594 Marquardt, J., X. Chen, and E. Bi. 2021. Septin Assembly and Remodeling at the Cell
595 Division Site During the Cell Cycle. *Front Cell Dev Biol*. 9:793920.

596 Martin-Cuadrado, A.B., J.L. Morrell, M. Konomi, H. An, C. Petit, M. Osumi, M.
597 Balasubramanian, K.L. Gould, F. Del Rey, and C.R. de Aldana. 2005. Role of
598 septins and the exocyst complex in the function of hydrolytic enzymes
599 responsible for fission yeast cell separation. *Molecular biology of the cell*.
600 16:4867-4881.

601 Mata, J., and P. Nurse. 1997. tea1 and the microtubular cytoskeleton are important for
602 generating global spatial order within the fission yeast cell. *Cell*. 89:939-949.

603 McCusker, D., and D.R. Kellogg. 2012. Plasma membrane growth during the cell cycle:
604 unsolved mysteries and recent progress. *Current opinion in cell biology*. 24:845-
605 851.

606 Mela, A., and M. Momany. 2022. Septins coordinate cell wall integrity and lipid
607 metabolism in a sphingolipid-dependent process. *Journal of cell science*. 135.

608 Merla, A., and D.I. Johnson. 2000. The Cdc42p GTPase is targeted to the site of cell
609 division in the fission yeast Schizosaccharomyces pombe. *European journal of*
610 *cell biology*. 79:469-477.

611 Mitchison, J.M., and P. Nurse. 1985. Growth in cell length in the fission yeast
612 Schizosaccharomyces pombe. *Journal of cell science*. 75:357-376.

613 Moreno, S., A. Klar, and P. Nurse. 1991. Molecular genetic analysis of fission yeast
614 Schizosaccharomyces pombe. *Methods in enzymology*. 194:795-823.

615 Munoz, S., E. Manjon, and Y. Sanchez. 2014. The putative exchange factor Gef3p
616 interacts with Rho3p GTPase and the septin ring during cytokinesis in fission
617 yeast. *The Journal of biological chemistry*. 289:21995-22007.

618 Murray, J.M., and D.I. Johnson. 2001. The Cdc42p GTPase and its regulators Nrf1p and
619 Scd1p are involved in endocytic trafficking in the fission yeast
620 Schizosaccharomyces pombe. *The Journal of biological chemistry*. 276:3004-
621 3009.

622 Okada, S., M. Leda, J. Hanna, N.S. Savage, E. Bi, and A.B. Goryachev. 2013. Daughter
623 cell identity emerges from the interplay of Cdc42, septins, and exocytosis.
624 *Developmental cell*. 26:148-161.

625 Onishi, M., T. Koga, A. Hirata, T. Nakamura, H. Asakawa, C. Shimoda, J. Bahler, J.Q.
626 Wu, K. Takegawa, H. Tachikawa, J.R. Pringle, and Y. Fukui. 2010. Role of septins
627 in the orientation of forespore membrane extension during sporulation in fission
628 yeast. *Molecular and cellular biology*. 30:2057-2074.

629 Onwubiko, U.N., P.J. Mlynarczyk, B. Wei, J. Habiyaremye, A. Clack, S.M. Abel, and
630 M.E. Das. 2019. A Cdc42 GEF, Gef1, through endocytosis organizes F-BAR
631 Cdc15 along the actomyosin ring and promotes concentric furrowing. *Journal of*
632 *cell science*. 132.

633 Ray, S., K. Kume, S. Gupta, W. Ge, M. Balasubramanian, D. Hirata, and D. McCollum.
634 2010. The mitosis-to-interphase transition is coordinated by cross talk between
635 the SIN and MOR pathways in Schizosaccharomyces pombe. *The Journal of cell*
636 *biology*. 190:793-805.

637 Revilla-Guarinos, M.T., R. Martin-Garcia, M.A. Villar-Tajadura, M. Estravis, P.M. Coll,
638 and P. Perez. 2016. Rga6 is a Fission Yeast Rho GAP Involved in Cdc42
639 Regulation of Polarized Growth. *Molecular biology of the cell*.

640 Rich-Robinson, J., A. Russell, E. Mancini, and M. Das. 2021. Cdc42 reactivation at
641 growth sites is regulated by local cell-cycle-dependent loss of its GTPase-
642 activating protein Rga4 in fission yeast. *Journal of cell science*. 134.

643 Rutkowski, D.M., V. Vincenzetti, D. Vavylonis, and S.G. Martin. 2024. Cdc42 mobility
644 and membrane flows regulate fission yeast cell shape and survival. *Nat*
645 *Commun*. 15:8363.

646 Singh, D., Y. Liu, Y.H. Zhu, S. Zhang, S. Naegele, and J.Q. Wu. 2024. Septins function
647 in exocytosis via physical interactions with the exocyst complex in fission yeast
648 cytokinesis. *bioRxiv*.

649 Sparks, C.A., M. Morphew, and D. McCollum. 1999. Sid2p, a spindle pole body kinase
650 that regulates the onset of cytokinesis. *The Journal of cell biology*. 146:777-790.

651 Spiliotis, E.T., and M.A. McMurray. 2020. Masters of asymmetry - lessons and
652 perspectives from 50 years of septins. *Molecular biology of the cell*. 31:2289-
653 2297.

654 Sprang, S. 2001. GEFs: master regulators of G-protein activation. *Trends in biochemical*
655 *sciences*. 26:266-267.

656 Tatebe, H., K. Nakano, R. Maximo, and K. Shiozaki. 2008. Pom1 DYRK regulates
657 localization of the Rga4 GAP to ensure bipolar activation of Cdc42 in fission
658 yeast. *Current biology : CB*. 18:322-330.

659 Verde, F., J. Mata, and P. Nurse. 1995. Fission yeast cell morphogenesis: identification
660 of new genes and analysis of their role during the cell cycle. *The Journal of cell*
661 *biology*. 131:1529-1538.

662 Wang, N., I.J. Lee, G. Rask, and J.Q. Wu. 2016. Roles of the TRAPP-II Complex and
663 the Exocyst in Membrane Deposition during Fission Yeast Cytokinesis. *PLoS*
664 *biology*. 14:e1002437.

665 Wang, N., M. Wang, Y.H. Zhu, T.W. Grosel, D. Sun, D.S. Kudryashov, and J.Q. Wu.
666 2015. The Rho-GEF Gef3 interacts with the septin complex and activates the
667 GTPase Rho4 during fission yeast cytokinesis. *Molecular biology of the cell*.
668 26:238-255.

669 Wei, B., B.S. Hercyk, J. Habiyaremye, and M. Das. 2017. Spatiotemporal Analysis of
670 Cytokinetic Events in Fission Yeast. *J Vis Exp*:e55109.

671 Wei, B., B.S. Hercyk, N. Mattson, A. Mohammadi, J. Rich, E. DeBruyne, M.M. Clark,
672 and M. Das. 2016. Unique Spatiotemporal Activation Pattern of Cdc42 by Gef1
673 and Scd1 Promotes Different Events during Cytokinesis. *Molecular biology of the*
674 *cell*. 27:1235-1245.

675 Woods, B.L., and A.S. Gladfelter. 2021. The state of the septin cytoskeleton from
676 assembly to function. *Current opinion in cell biology*. 68:105-112.

677 Zheng, S., B. Zheng, Z. Liu, X. Ma, X. Liu, X. Yao, W. Wei, and C. Fu. 2022. The Cdc42
678 GTPase-activating protein Rga6 promotes the cortical localization of septin.
679 *Journal of cell science*. 135.
680

681 **Figure Legends**

682 **Figure 1. The septin cytoskeleton restricts Rga4 to the cell sides during**
683 **interphase. A.** Middle plane images of Rga4-GFP in *spn1*$^{+}$ and *spn1Δ* cells. Red
684 brackets highlight Rga4 distribution along cell sides in interphase cells. Red asterisks
685 highlight dividing cells. **B-C**. Quantification of the coefficient of variation of Rga4
686 distribution through the cell-cycle in *spn1*$^{+}$ (B) and *spn1Δ* (C) cells. [N=3, *n*=40-50 cells
687 each, **P*≤0.05, *ns*=not significant,]. **D.** Rga4-GFP increasingly localizes to the cell ends
688 and cytoplasm in *spn1Δ* cells during interphase. Images consist of superimposed
689 middle-plane images taken at 10 second intervals over 5 minute timelapse. Red boxes
690 highlight increased localization of Rga4 to the cell ends. **E.** Quantification of Rga4-GFP
691 intensity within the cytoplasm of interphase cells in *spn1*$^{+}$ and *spn1Δ* conditions
692 measured by averaging three unique regions within the cytoplasm of each cell [
693 ***P*≤0.01, Student's T test]. **F.** Quantification of Rga4-GFP localization to growing and
694 non-growing cell ends of interphase cells in *spn1*$^{+}$ and *spn1Δ* conditions. [N=3, *n*=24-28
695 cells each, *****P*≤0.0001, ****P*≤0.001, ***P*≤0.01, **P*≤0.05, *ns*=not significant, one-way
696 ANOVA, scale bar=5μm].

697

698 **Figure 2. Septins inhibit Rga4-GFP mobility along the plasma membrane during**
699 **Interphase. A.** Montage of Rga4-GFP in *spn1*$^{+}$ cells during interphase, during mitosis,
700 and in *spn1Δ* cells during interphase, taken over 5 minute timelapse. Red arrowhead
701 marks an Rga4-GFP puncta. **B.** Montage of Rga4-GFP recovery after photobleaching
702 during interphase and mitosis in *spn1*$^{+}$ and *spn1Δ* cells taken in 15 second intervals.
703 Red circles indicate the photobleached region of interest (ROI). Red lightning bolt

704 indicates the timepoint of photobleaching. **C.** FRAP recovery rates of Rga4-GFP signal
705 intensity within the ROI over time in *spn1*$^{+}$ and *spn1Δ* cells during interphase and
706 mitosis. **D.** $T_{1/2}$ fluorescence recovery times of listed conditions. [N=3, *n*=10 cells each,
707 ***P*≤0.01, **P*≤0.05, *ns*=not significant, one-way ANOVA, scale bar=5μm].
708
709 **Figure 3. Septins form linear filaments along the cell sides in interphase and a**
710 **ring at the division site as Anaphase B ends. A.** Spn3-GFP and Spn1-tdT colocalize
711 in linear filaments along the cell cortex during interphase, and within a ring during
712 division. Red and white arrowheads highlight filaments. **B.** Spn2-GFP show linear
713 filament like organization along the cell sides during interphase and a ring at the division
714 site during mitosis. Red arrowhead marks a filament. **C.** Spn4-tdTomato localize along
715 the cell sides during interphase in a punctate pattern and form a ring at the division site
716 during mitosis. Red arrowhead marks punctate organization. **D.** Montage of timelapse of
717 Spn4-tdTomato and Moyo2-GFP Sid4-GFP expressing cells during mitosis. Red asterisk
718 marks onset of mitosis, the green asterisk marks onset of septin ring formation and
719 purple asterisk marks end of mitosis. **E.** Quantification over time of Spn4-TdTomato
720 levels along the cell side of the cell shown in D. F. Quantification of Spn4-tdTomato
721 along the cell sides with increasing spindle pole body distances. [N=3, n=>20, **P*≤0.05,
722 one-way ANOVA, scale bar=5μm or 2μm as indicated]
723
724 **Figure 4. The septin cytoskeleton does not colocalize or interact with Rga4.** A.
725 Rga4-GFP and Spn1-tdTomato show distinct localization pattern along the sides of
726 interphase cells. Red arrowhead zones with Rga4-GFP but no Spn1-tdTomato along the

727 cell side. Middle plane inset shows partial colocalization of Rga4-GFP with Spn1-
728 tdTomato. Top plane inset shows distinct localization patterns of these proteins. **B.**
729 Spn3-GFP mislocalizes to Tom20-GBP-RFP at the mitochondria. **C.** Spn3-GFP and
730 Spn1-tdT simultaneously mislocalize to the mitochondria in Tom20-GBP expressing
731 cells. **D.** Rga4-GFP mislocalizes to the mitochondria, but not Spn1-tdT in Tom20-GBP
732 expressing cells. **E.** Spn3-GFP mislocalizes to the mitochondria, but not Rga4-mCh in
733 Tom20-GBP expressing cells. **F.** Quantification of the coefficient of variation of Rga4-
734 mCherry distribution along cell sides in interphase cells, Spn3-GFP and Tom20-GBP
735 expressing cells as shown in E. [N=3, *n*=20-26 cells each, *$P \leq 0.05$, student's t-test,
736 scale bar=5μm].
737
738 **Figure 5. As septins recede from the cell sides, Rga4 spreads out along the**
739 **membrane and Cdc42 activity diminishes at the cell ends. A.** A representative
740 timelapse of Spn3-GFP, CRIB-mCherry and Sad1-mCherry expressing cells starting at
741 the onset of mitosis. B. A representative timelapse of CRIB-3xGFP and Rlc1tdTomato in
742 *spn1*$^{+}$ and *spn1Δ* cells. Red asterisk marks onset of stable CRIB-3xGFP localization at
743 the cell ends after the completion of ring constriction marked with a purple asterisk. **C.**
744 Frequency plot of the timing of loss of active Cdc42 (CRIB-mCherry) from the cell ends,
745 septin ring formation and end of Anaphase B with respect to the onset of mitosis.
746 (n=10). **D.** Frequency plot of the timing of the onset of stable Cdc42 activity at the cell
747 ends as indicated by CRIB-3xGFP after the completion of ring constriction in *spn1*$^{+}$ and
748 *spn1Δ* cells (n>30). Scale bar=5μm.
749

750 **Figure 6. The septin cytoskeleton promotes bipolar growth. A.** Representative
751 images of calcofluor white-stained *spn1*$^{+}$ and *spn1Δ* cells. Red asterisks highlight
752 bipolar (*spn1*$^{+}$) and monopolar (*spn1Δ*) growth. **B.** Quantification of monopolarity index
753 in *spn1*$^{+}$ and *spn1Δ* cells. **C.** Quantification of cell width in *spn1*$^{+}$ and *spn1Δ* cells. [N=3,
754 *n*=65-100 cells each, **P*≤0.05, student's t-test]. **D.** Representative Maximum Z-
755 Projection images of *spn1*$^{+}$ and *spn1Δ* cells expressing CRIB-GFP. Red arrowheads
756 highlight Cdc42 activity at the ends of growing cells. **E.** Quantification of CRIB-GFP
757 intensity at growing cell ends in *spn1*$^{+}$ and *spn1Δ* cells. **F.** Quantification of the length of
758 CRIB-GFP cap at growing cell ends in *spn1*$^{+}$ and *spn1Δ* cells. [N=3, *n*=65-100 cells
759 each, **P*≤0.05, ***P*≤0.01, student's t-test]. **G.** Heat map of the fraction of CRIB-GFP
760 intensity at each cell end over the total intensity with increasing cell size in *spn1*$^{+}$ and
761 *spn1Δ* cells. **H, I.** Quantification of Scd1-mNG and Scd2-GFP at the ends of *spn1*$^{+}$ and
762 *spn1Δ* cells [N=3, *n*=65-100 cells each, **P*≤0.05, ***P*≤0.01, student's t-test]. **J,K.**
763 Representative images of Scd1-mNG and Scd2-GFP (Red arrowheads) at the ends of
764 *spn1*$^{+}$ and *spn1Δ* cells. scale bar=5μm

Figure 1

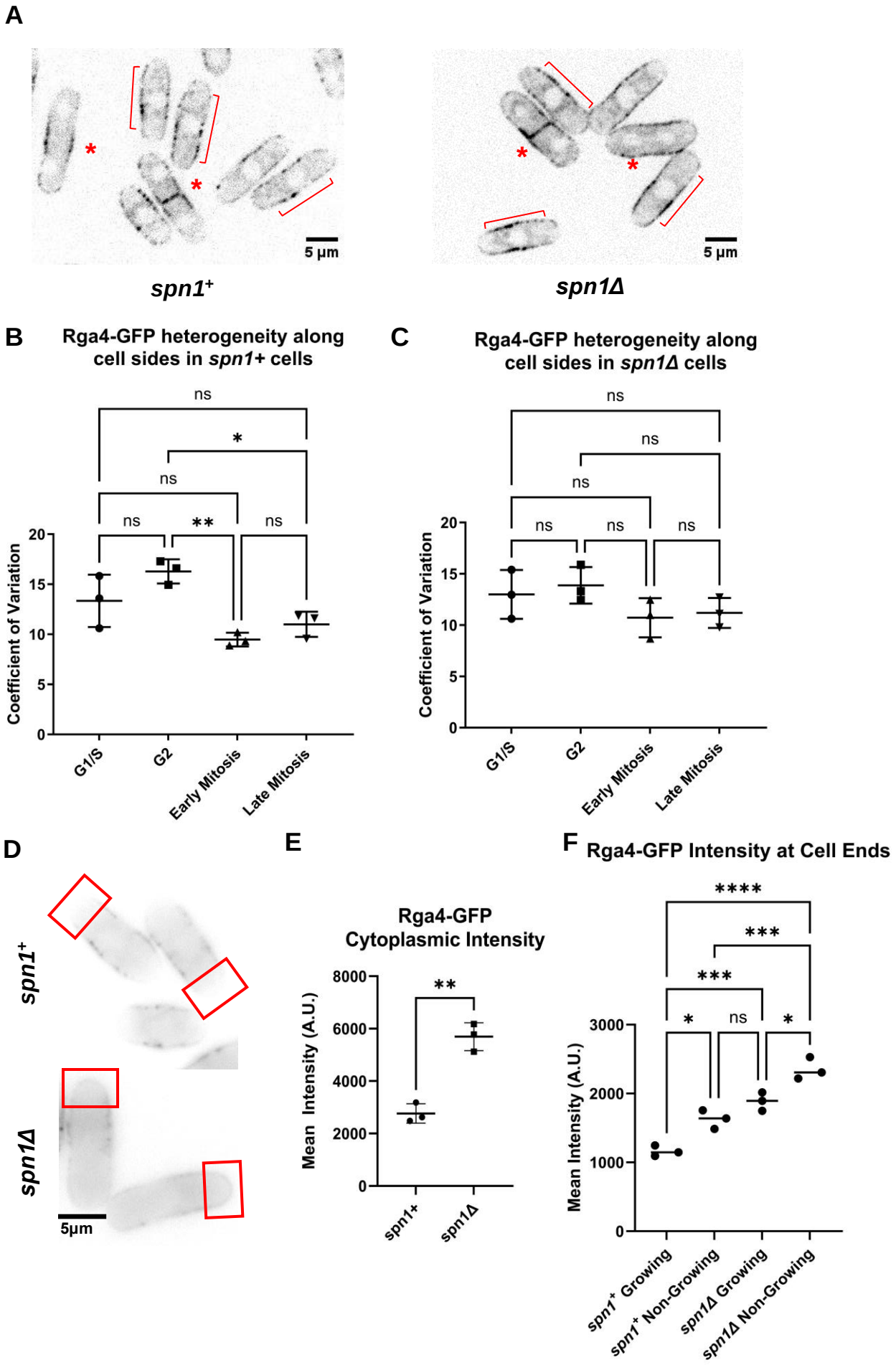
A
5 µm
spn1+
spn1Δ
B
Rga4-GFP heterogeneity along cell sides in spn1+ cells
Coefficient of Variation
G1/S
G2
Early Mitosis
Late Mitosis
C
Rga4-GFP heterogeneity along cell sides in spn1Δ cells
D
5µm
E
Rga4-GFP Cytoplasmic Intensity
Mean Intensity (A.U.)
F
Rga4-GFP Intensity at Cell Ends
spn1+ Growing
spn1+ Non-Growing
spn1Δ Growing
spn1Δ Non-Growing

Figure 2

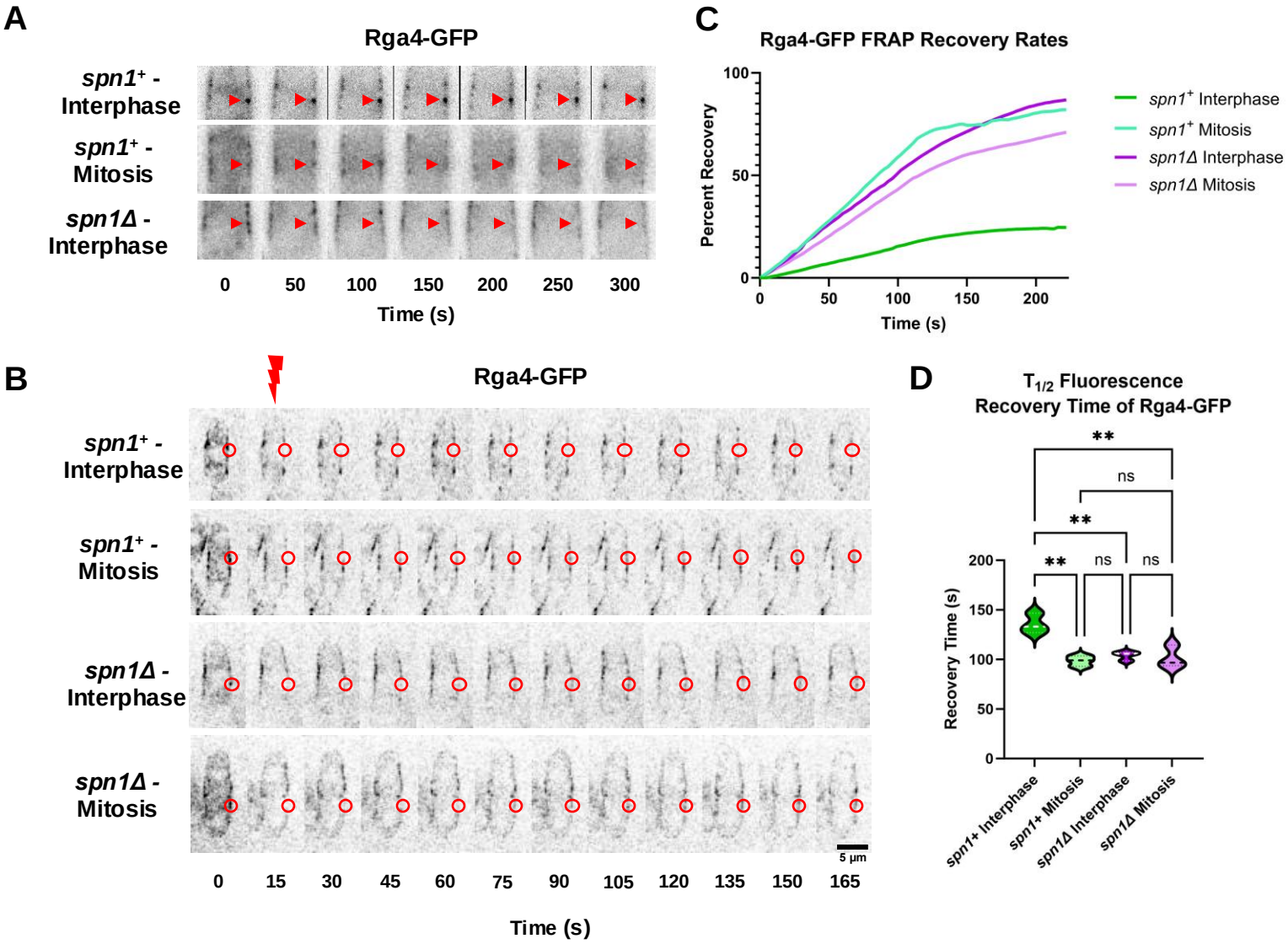
A
Rga4-GFP
spn1+ - Interphase
spn1+ - Mitosis
spn1Δ - Interphase
0
50
100
150
200
250
300
Time (s)
C
Rga4-GFP FRAP Recovery Rates
Percent Recovery
100
50
0
0
50
100
150
200
Time (s)
spn1+ Interphase
spn1+ Mitosis
spn1Δ Interphase
spn1Δ Mitosis
B
Rga4-GFP
spn1+ - Interphase
spn1+ - Mitosis
spn1Δ - Interphase
spn1Δ - Mitosis
5 µm
0
15
30
45
60
75
90
105
120
135
150
165
Time (s)
D
T1/2 Fluorescence Recovery Time of Rga4-GFP
Recovery Time (s)
200
150
100
50
0
**
ns
**
**
ns
ns
spn1+ Interphase
spn1+ Mitosis
spn1Δ Interphase
spn1Δ Mitosis

Figure 3.

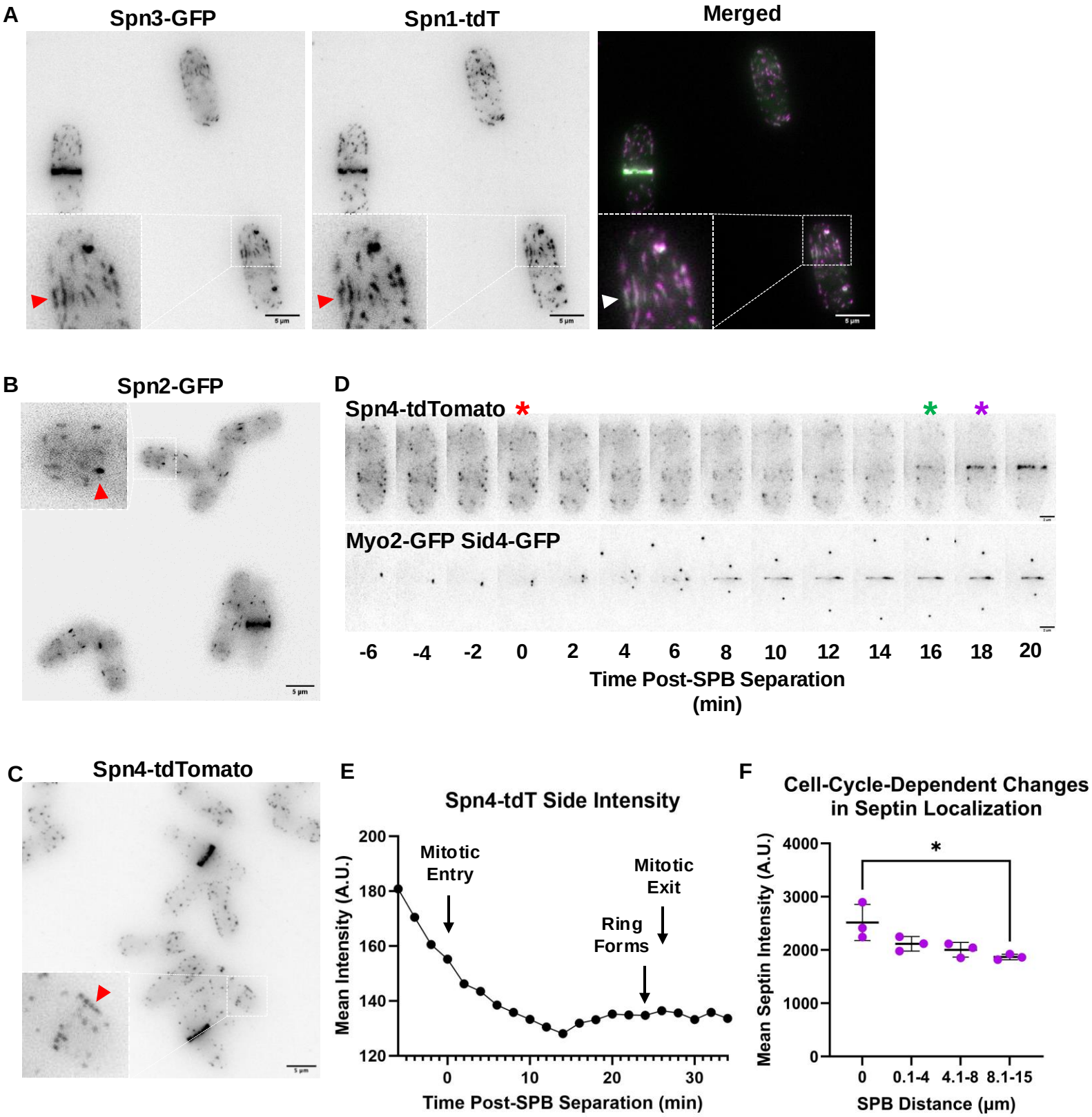
A
Spn3-GFP
Spn1-tdT
Merged
B
Spn2-GFP
D
Spn4-tdTomato
Myo2-GFP Sid4-GFP
-6 -4 -2 0 2 4 6 8 10 12 14 16 18 20
Time Post-SPB Separation (min)
C
Spn4-tdTomato
E
Spn4-tdT Side Intensity
Mitotic Entry
Mitotic Exit
Ring Forms
Mean Intensity (A.U.)
200 180 160 140 120
0 10 20 30
Time Post-SPB Separation (min)
F
Cell-Cycle-Dependent Changes in Septin Localization
Mean Septin Intensity (A.U.)
4000 3000 2000 1000 0
0 0.1-4 4.1-8 8.1-15
SPB Distance (µm)

Figure 4.

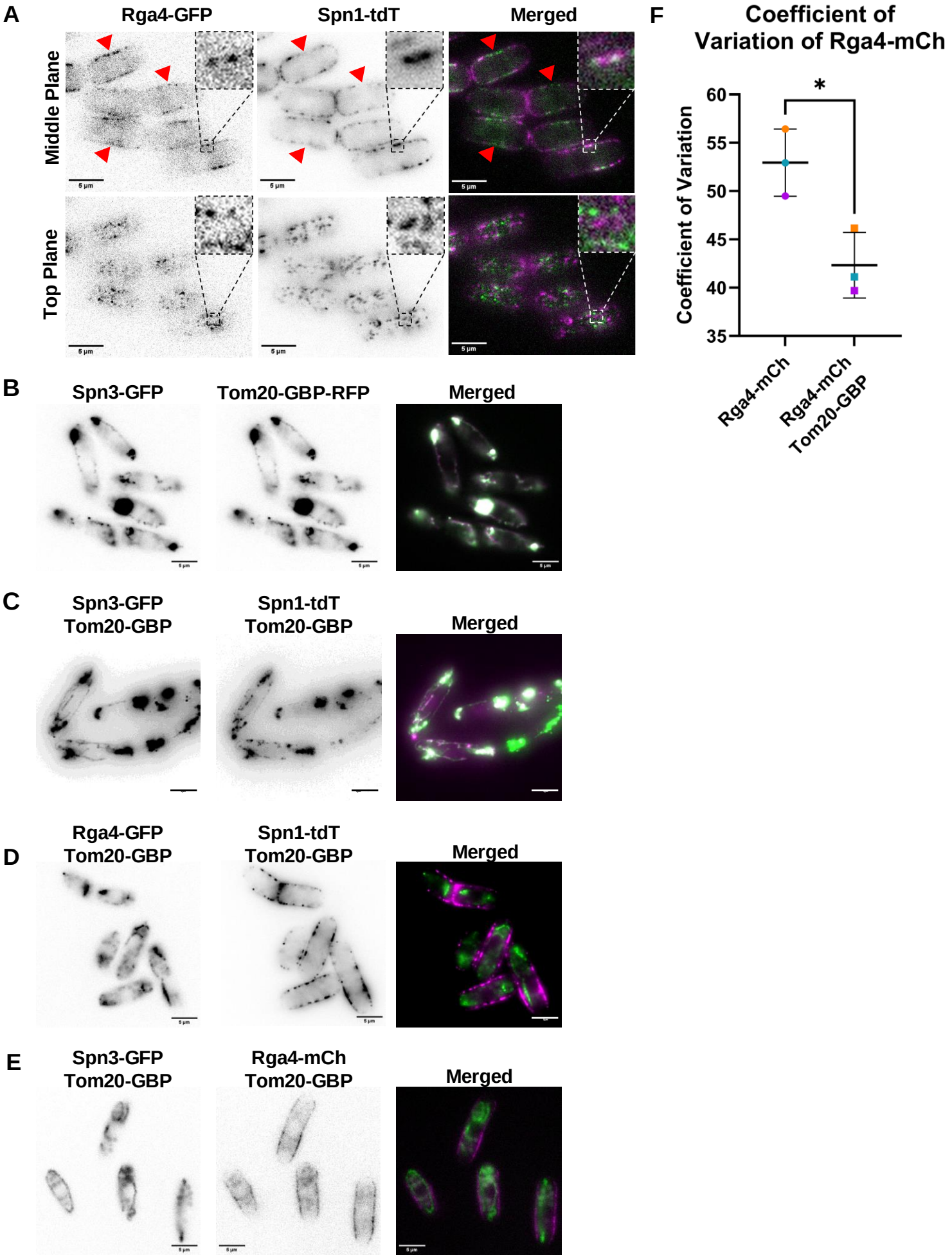
A
Rga4-GFP
Spn1-tdT
Merged
Middle Plane
Top Plane
B
Spn3-GFP
Tom20-GBP-RFP
Merged
C
Spn3-GFP
Tom20-GBP
Spn1-tdT
Tom20-GBP
Merged
D
Rga4-GFP
Tom20-GBP
Spn1-tdT
Tom20-GBP
Merged
E
Spn3-GFP
Tom20-GBP
Rga4-mCh
Tom20-GBP
Merged
F
Coefficient of Variation of Rga4-mCh
Coefficient of Variation
60
55
50
45
40
35
*
Rga4-mCh
Rga4-mCh
Tom20-GBP

Figure 5.

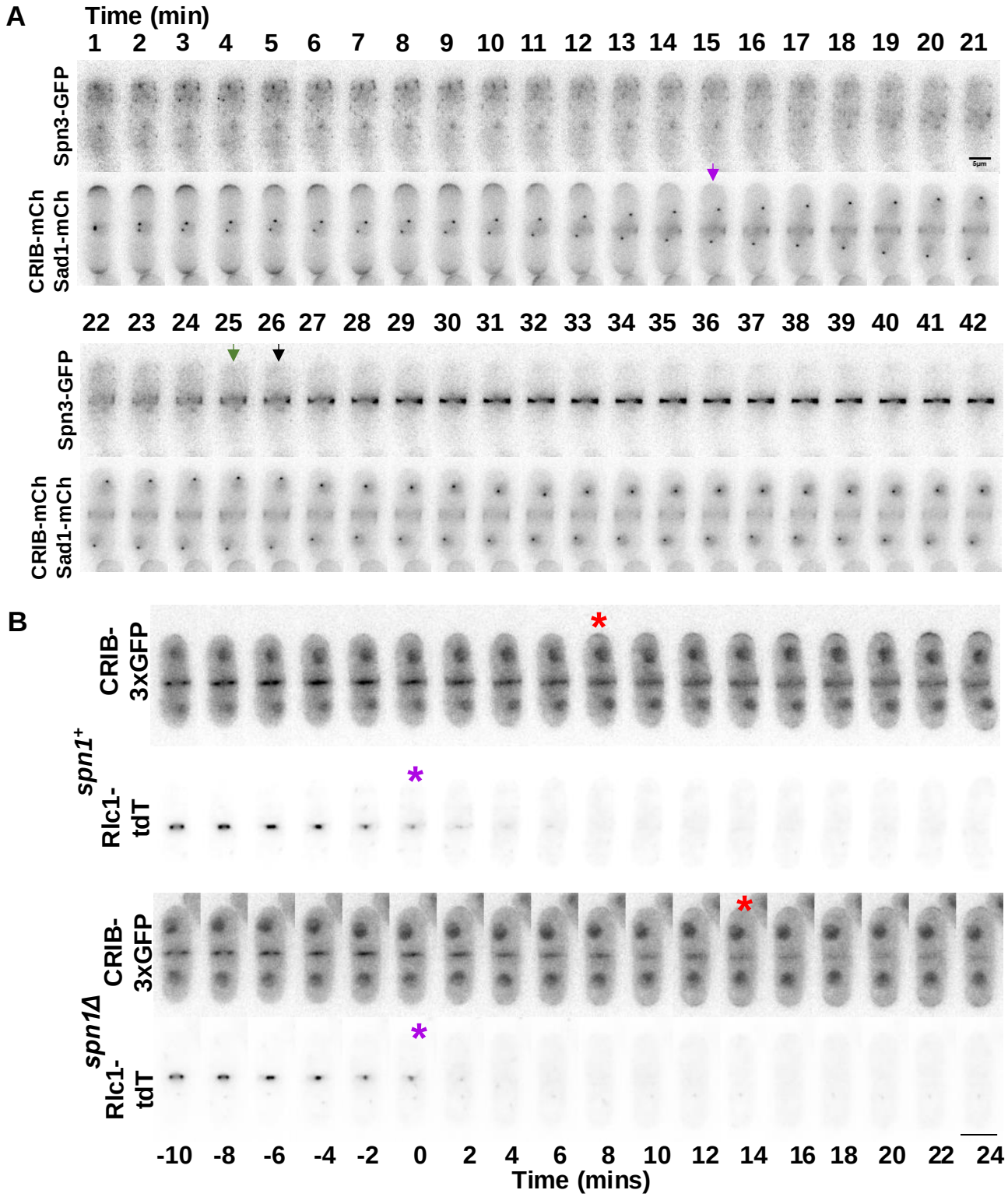
A
Time (min)
1 2 3 4 5 6 7 8 9 10 11 12 13 14 15 16 17 18 19 20 21
Spn3-GFP
CRIB-mCh
Sad1-mCh
22 23 24 25 26 27 28 29 30 31 32 33 34 35 36 37 38 39 40 41 42
Spn3-GFP
CRIB-mCh
Sad1-mCh
B
CRIB-3xGFP
spn1+
Rlc1-tdT
CRIB-3xGFP
spn1Δ
Rlc1-tdT
-10 -8 -6 -4 -2 0 2 4 6 8 10 12 14 16 18 20 22 24
Time (mins)

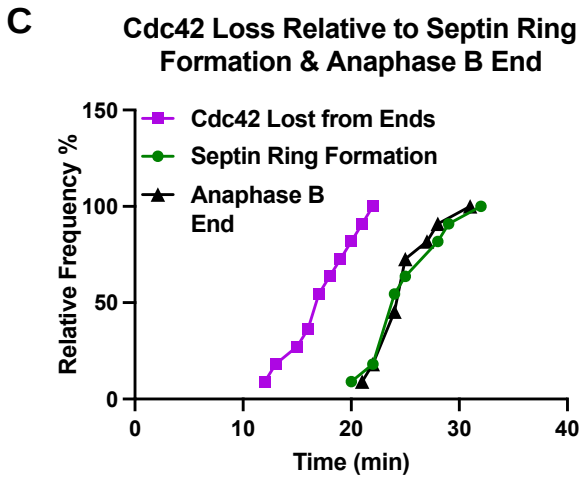
C
Cdc42 Loss Relative to Septin Ring Formation & Anaphase B End
Cdc42 Lost from Ends
Septin Ring Formation
Anaphase B End
Relative Frequency %
150
100
50
0
0 10 20 30 40
Time (min)

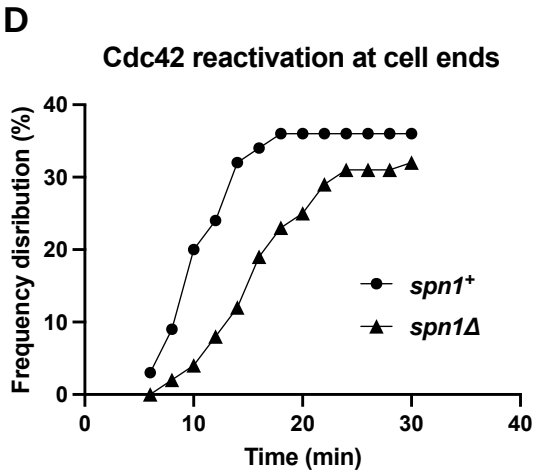
D
Cdc42 reactivation at cell ends
Frequency disribution (%)
40
30
20
10
0
0 10 20 30 40
Time (min)
spn1+
spn1Δ

Figure 6.

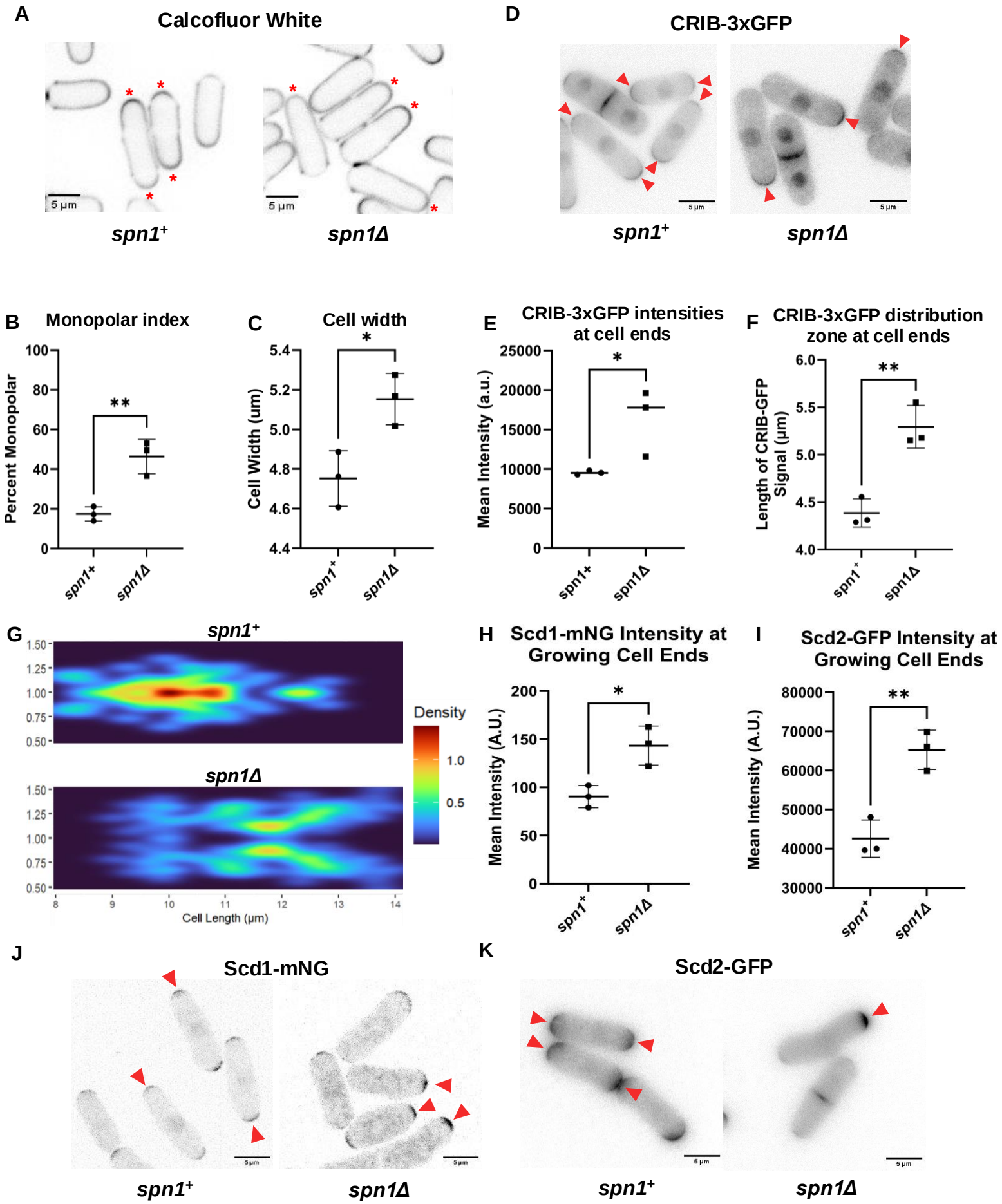
A
Calcofluor White
5 µm
5 µm
spn1+
spn1Δ
D
CRIB-3xGFP
5 µm
5 µm
spn1+
spn1Δ
B
Monopolar index
Percent Monopolar
100
80
60
40
20
0
**
spn1+
spn1Δ
C
Cell width
Cell Width (um)
5.4
5.2
5.0
4.8
4.6
4.4
*
spn1+
spn1Δ
E
CRIB-3xGFP intensities at cell ends
Mean Intensity (a.u.)
25000
20000
15000
10000
5000
0
*
spn1+
spn1Δ
F
CRIB-3xGFP distribution zone at cell ends
Length of CRIB-GFP Signal (µm)
6.0
5.5
5.0
4.5
4.0
**
spn1+
spn1Δ
G
spn1+
1.50
1.25
1.00
0.75
0.50
spn1Δ
1.50
1.25
1.00
0.75
0.50
8
9
10
11
12
13
14
Cell Length (µm)
Density
1.0
0.5
H
Scd1-mNG Intensity at Growing Cell Ends
Mean Intensity (A.U.)
200
150
100
50
0
*
spn1+
spn1Δ
I
Scd2-GFP Intensity at Growing Cell Ends
Mean Intensity (A.U.)
80000
70000
60000
50000
40000
30000
**
spn1+
spn1Δ
J
Scd1-mNG
5 µm
5 µm
spn1+
spn1Δ
K
Scd2-GFP
5 µm
5 µm
spn1+
spn1Δ